Design and Implementation of Active Power Control with Improved P&O Method for Wind-PV-Battery based Standalone Generation System

M. Rezkallah, *IEEE Member*, A. Hamadi, A. Chandra, *Fellow, IEEE* and B. Singh *Fellow, IEEE*

***Abstract*— In this paper, the design and implementation of active power control (APC) with anti-windup PI controller (AWPI) and improved perturbation and observation (P&O) method with sliding mode control (SMC), are investigated to get high level of performance with reduced number of sensors for a stable operation of a wind-PV-battery based hybrid standalone power generation system (HSPGS). The SMC approach with boundary layer, is used to have an optimum trajectory of the system as sliding manifold of surfaces, under variable operating conditions of many power converters operated in simultaneously. Furthermore, detailed modeling and stability analysis to demonstrate the transversality, reachability and equivalent control, are presented. The effectiveness and robustness of HSPGS and their respective control strategies are validated by simulation and test results on a hardware prototype using DSP-dSPACE real time controller.**

.

***Index Terms*— Hybrid standalone power generation system (HSPGS), wind turbine (WT), solar photovoltaic array (SPVA), sliding mode control (SMC), stability analysis, perturbation & observation method (P&O), anti-windup PI controller (AWPI), active power control (APC).**

I. INTRODUCTION

SEVERAL remote areas in the world use only diesel generators (DGs) to support their electricity needs. This energy source (ES) is costly and pollutant. However, hybrid standalone power generation system (HSPGS) based on wind and solar energy supported by the battery energy storage system (BESS) is considered as a promising solution for remote areas to reduce diesel-fuel dependency, to minimize the greenhouse (GHS) emissions, to reduce power transmission, and to minimize the system losses [1]. This new technology is effective however, it requires improvement especially in the design and control to become simple and easy to use.

ESs are proposed in the literature [2]. In the most of the proposed configurations [3,4], multi-stage converters are used to connect the distributed energy resources (DERs) to the point of common coupling (PCC), which leads to an increase of energy losses and the cost of installation. In [5], AC-DC microgrid configuration is proposed to connect the DERs to the PCC. The authors have succeeded to achieve their objectives; however, this proposition is not validated in real-time. Generally, single or two-stage converters are used to connect the PCC and the solar photovoltaic array (SPVA) [6]. In [7], a single stage system is proposed and obtained results show satisfactory performance. According to [7-9] and the comparative study realized in [10], two stage system shows high level of performance especially in DC voltage stability and power quality.

Regarding, the efficiency of SPVA and WT, many methods are developed in the literature to track the maximum power point (MPP) [11, 12]. Compared to the existing MPP tracking (MPPT) methods, perturbation and observation (P&O) is extensively applied as an easy method. Unfortunately, this method suffers from the continuous oscillation that occurs around the MPP. In addition, it loses the tracking direction during sudden change in weather conditions. These drawbacks are solved in [13] by limiting the control using dynamic boundary conditions. This solution is effective however, it requires improvement especially in modeling and stability analysis. In [14], an improved beta-P&O method is proposed to solve the drawbacks of the classical P&O method. This solution is complex and its dynamics is slow. Furthermore, it requires large run time because it uses two stages, 1) adaptive scaling factor beta to get high level of performance during transient response, and 2) zero oscillations P&O method for steady-state error. Similarly, the authors in [14-15], have presented improvement in the performance of classical P&O by using delta-P&O, PI-P&O, as well as, ZA-P&O methods, however, with complicated control and hardware complexity. In the same context, hybrid analog-digital sliding mode

Manuscript received May 10, 2017; revised September 20, 2017 and May 4, 2016; accepted October 22, 2017. This work was supported in part by the Natural Sciences and Engineering Research Council of Canada (NSERC).

M. Rezkallah, A. Hamadi and A. Chandra are with the Electrical Engineering Department, École de Technologie Supérieure, 1100 Notre-Dame Montréal, Québec H3C1K3 Canada (miloud.rezkallah.1@ens.etsmtl.ca,abdelhamidhamadi@yahoo.fr;ambrish.chandra@etsmtl.ca).

B.Singh is with the Electrical Engineering Department, Indian Institute of Technology Delhi, New Delhi-110016, India. (bsingh@ee.iitd.ac.in).

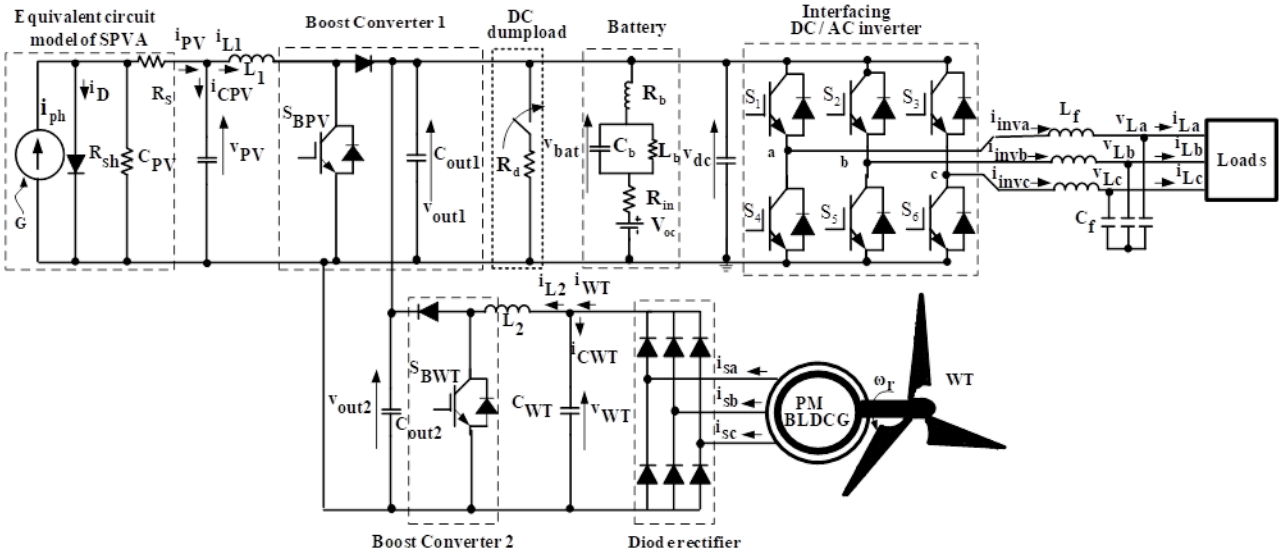

Fig. 1. HSPGS configuration under study.

controller (SMC) is presented for P&O method in [16] to achieve high performance especially during weather changes, and for fast tracking, the P&O based SMC is used in [17]. In [18], the tip-speed ratio based SMC has been proposed for variable speed WT. The same approach is applied in [19-21] with detailed stability analysis and controller gains calculation. In all these studies [9],[16-21], successful validation of SMC based MPPT for SPVA and variable speed WT, on hardware prototype is presented and obtained results show satisfactory performance. However, these SMC based MPPT methods [9],[16-21], are applied and validated for simple systems using only one DER with reduced number power converters, where the chattering phenomenon due to high switching frequency is not a big issue.

In a HSPGS, voltage and frequency are regulated by controlling the DC-AC interfacing inverter using appropriate control strategy such as, adaptive voltage control [22] or the new fuzzy adaptive voltage controller [23]. The presented results have shown satisfactory performance however, they require additional sensors and are complex to implement. In the same context, improved droop control strategy is suggested in [24-28] for easy implementation in real time. Unfortunately, in all proposed control strategies [24-28], the inner and outer loops are used in classical PI controllers and the saturation limits are considered, which is not enough to prevent wind-up when the system exceeds its physical limits. In such cases, the feedback loop is broken and the system runs as an open loop.

Inspired from these previous studies, an improved P&O based SMC with boundary layer, is proposed in this work to achieve improved performance with stable operation from SPVA and WT, with less concerns of chattering phenomenon when many power converters operate simultaneously. Furthermore, new solution to achieve MPPT from WT without any wind speed or rotor position sensors, is proposed to reduce the hardware complexity, and detailed stability analysis is presented. Active power control (APC) with reduced number of current sensors is proposed for voltage regulation at the PCC. In addition, to avoid the saturation phenomenon and to prevent voltage overshoot during transitions, an AWPI voltage controller with optimal gain design is proposed here.

II. System Configuration

Fig.1 shows the proposed HSPGS configuration for isolated areas that possess a good wind and solar potential. It consists of SPVA, WT driven variable speed permanent magnet brushless DC generator (PMBLDCG), BESS, two boost converters, a three-phase diode rectifier, interfacing DC-AC power inverter, LC low-pass filter, loads, and a DC dump load. To avoid the synchronization issues, all DERs are connected to the DC bus. Three control strategies are developed to ensure stable and affective operation of HSPGS under sever conditions.

III. Modeling and Control Strategies

In this section, modeling and developed control strategies for boost power converters of SPVA and WT, and an interfacing three-phase power inverter, as well as, the stability analysis, are given in detail.

A. Modeling and control design for SPVA

From Fig.1, a boost converter of SPVA, is modeled as follows.

$$L_1\left(\partial i_{L1}/\partial t\right)=v_{PV} \tag{1}$$

$$C_{out1}\left(\partial v_{out1}/\partial t\right)=-v_{out1}/R \tag{2}$$

$$i_{CPV}=C_{PV}\left(\partial v_{CPV}/\partial t\right)=i_{PV}-i_{L1} \tag{3}$$

And for S_{BPV}=0 (OFF),

$$L_1\left(\partial i_{L1}/\partial t\right)=v_{PV}-v_{out1} \tag{4}$$

$$C_{out1}\left(\partial v_{out1}/\partial t\right)=i_{L1}-\left(v_{out1}/R\right) \tag{5}$$

where S_{BPV}, L_1, C_{PV}, C_{out1}, R, i_{L1}, i_{PV}, i_{CPV}, v_{out1}, and v_{CPV} represent the switch, inductance, input and output capacitances, equivalent load resistance, inductor current, output PV current, input capacitor current, output voltage, and input capacitor voltage of the boost converter1, respectively.

Based on (1) to (5), the following equations for boost converter 1, are obtained as,

$$\left(\partial i_{L1}/\partial t\right)=\left(v_{PV}/L_1\right)-\left(1-d_1\right)\left(v_{out1}/L_1\right) \tag{6}$$

$$\left(\partial v_{out1}/\partial t\right)=\left(1/C_{out1}\right)\left[\left(i_{L1}\left(1-d_1\right)\right)-\left(v_{out1}/R\right)\right] \tag{7}$$

Rearranging (6), one gets the following expression as,

$$\left(\partial i_{PV}/\partial t\right)=\overbrace{\left(v_{PV}/L_1\right)-\left(1-d_1\right)\left(v_{out1}/L_1\right)}^{Term1}+\overbrace{C_{PV}\left(\partial^2 v_{PV}/\partial t^2\right)}^{Term2} \tag{8}$$

where d_1 is the desired control.

The variation of the v_{PV} during court duration is equal to zero. However, the second derivative of v_{PV} is equal to zero. Hence, expression given in (8) becomes as follows,

$$\left(\partial i_{PV}/\partial t\right)=\left(v_{PV}/L_1\right)-\left(1-d_1\right)\left(v_{out1}/L_1\right) \tag{9}$$

1) Control strategy for the Boost converter-1

Fig.2 shows the control scheme of the improved P&O method based on SMC with boundary layer, which is used to achieve high performance from SPVA and to ensure the stability during sudden change in solar insolation in finite time.

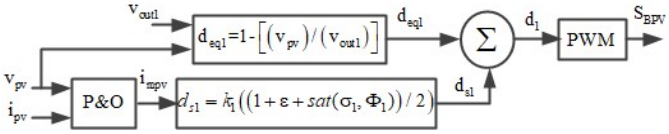

Fig. 2. Improved P&O based SMC with boundary layer for SPVA.

The design of SMC is based on the following steps;

2) Sliding surface selection

To reach the surface and achieve MPPT without loss of the control, sliding surface σ_1 is selected as:

$$\sigma_1=\left(\partial P_{PV}/\partial i_{PV}\right)=0 \tag{10}$$

where P_{PV} denotes the generated power from SPVA and it is equal to,

$$P_{PV}=v_{PV}i_{PV} \tag{11}$$

Replacing (11) in (10), one obtains,

$$\sigma_1=\left(\partial P_{PV}/\partial i_{PV}\right)=\partial\left(v_{PV}i_{PV}\right)/\partial i_{PV} \tag{12}$$

Rearranging (12), one gets the following expression,

$$\sigma_1=v_{PV}+i_{mPV}\left(\partial v_{PV}/\partial i_{mPV}\right) \tag{13}$$

where i_{mPV} denotes the optimal output PV current obtained using the classical P&O method [29].

3) Model of the equivalent control

To reach the surface and achieve MPPT without loss of the control, sliding surface σ_1 is selected as:

The equivalent control is obtained by setting the derivative of (13) to zero.

The structure of the chosen control (d_1) is expressed as,

$$d_1=d_{eq1}+d_{s1} \tag{14}$$

And the switching control (d_{s1}) is defined as,

$$d_{s1}=k_1\left(\left(1+\varepsilon+sat(\sigma_1,\Phi_1)\right)/2\right) \tag{15}$$

With

$$sat\left(\sigma_1,\Phi_1\right)\begin{cases}1 & \sigma_1\succ\Phi_1\\ \sigma_1/\Phi_1 & \left|\sigma_1\right|\le\Phi_1\\ -1 & \sigma_1\prec-\Phi_1\end{cases} \tag{16}$$

where k_1 d_{eq1}, ε and Φ_1, denote positive control gain, equivalent control, very small value and sliding layer, which is chosen to be between 0.5 and -0.5.

$$\begin{aligned}\left(\partial\sigma_1/\partial t\right)&=\left(\partial\sigma_1/\partial i_{mPV}\right)\left(\partial i_{mPV}/\partial t\right)\\&=\left(\partial\sigma_1/\partial i_{mPV}\right)\left[\left(v_{PV}/L_1\right)-\left(1-d_1\right)\left(v_{out1}/L_1\right)\right]\end{aligned} \tag{17}$$

The non-trivial solution of (17) is described as follows,

$$v_{PV}-\left(1-d_1\right)v_{out1}=0 \tag{18}$$

The equivalent control is obtained from (18) as,

$$deq_1=1-\left(v_{PV}/v_{out1}\right) \tag{19}$$

4) System stability analysis

The Lyapunov function candidate is used to verify the system stability as,

$$V_1=\left(1/2\right)\sigma_1^{\,2} \tag{20}$$

The system is globally stable if the derivative of (20) is negative as.

$$\left(\partial V_1/\partial t\right)=\sigma_1\left(\partial\sigma_1/\partial t\right)\langle 0 \tag{21}$$

Replacing (13) and (17) into (21) gives (22), which consists of three terms as,

$$\overbrace{\left(v_{PV}+i_{mPV}\left(\partial v_{PV}/\partial i_{mPV}\right)\right)}^{Term1}\overbrace{\left(2\left(\partial v_{PV}/\partial i_{mPV}\right)+i_{mPV}\left(\partial^2 v_{PV}/\partial^2 i_{mPV}\right)\right)}^{Term2}\overbrace{\left(\left(v_{PV}/L_1\right)-\left(1-d_1\right)\left(v_{out1}/L_1\right)\right)}^{Term3}\langle 0 \tag{22}$$

where, v_{PV} denotes the output PV voltage, and is expressed as,

$$v_{PV}=\left(k_bTA/q\right)\ln\left(\left(i_{ph}+i_D-i_{L1}\right)/i_D\right) \tag{23}$$

where, k_b, T, A, q, i_{ph}, i_D, i_L, denote Boltzmann's constant, cell temperature, ideality factor, charge of an electron, light-generated current, saturation and the PV currents, respectively.

It is observed in (22) that $term_1$ and $term_2$ contain the 1st and the 2nd derivatives of output PV voltage (v_{PV}). To verify the sign of (21), we replace the 1st and 2nd derivatives of v_{PV} given in (24) and (25) into (22) are replaced as fellows.

The 1st and 2nd derivatives of v_{PV}, are described as,

$$\left(\partial v_{PV}/\partial i_{L1}\right)=-\overbrace{\left(k_bTA/q\right)}^{Term1}\overbrace{\left(i_D/\left(i_{ph}+i_D-i_{L1}\right)\right)}^{Term2} \tag{24}$$

$$\left(\partial^2 v_{PV}/\partial^2 i_{L1}\right)=-\overbrace{\left(k_bTA/q\right)}^{Term1}\overbrace{\left(i_D/\left(i_{ph}+i_D-i_{L1}\right)^2\right)}^{Term2} \tag{25}$$

To verify the stability condition defined in (21), signs of all terms in (22) must be determined. Light generated current (i_{ph}) in $term_2$ of (23) is greater than the saturation current (i_D) and the inductor current (i_{L1}). However, $term_2$ is smaller and positive. The sign of the $term_1$ of (22) is positive and its value, which is calculated using real parameters of SPVA given in Table II, is equal to (k_bTA/q=0.0026).

The sign of $term_1$ of (22) is positive, this is due the output PV voltage v_{PV}, which is greater than the value of term ($i_{mPV}(\partial v_{PV}/\partial i_{imPV})$). The sign of $term_2$, which is negative, is deduced using the sign of the 1st and the 2nd derivative of v_{PV}, which are already calculated in (24) and (25). Based on the obtained results, sign of $term_3$ in (22) must be positive to

verify the stability conditions given in (21). Replacing (19) in (14) and after in $term_3$ of (22), gives the following expression,

$$\left(\overbrace{\left(v_{out1} / L_1\right)}^{Term1} k_1 \overbrace{\left(\left(1+\varepsilon+sat(\sigma_1,\Phi_1)\right)/2\right)}^{x1} \right) \overbrace{\qquad\qquad}^{Term2} \rangle 0 \tag{26}$$

$Term_1$ in (26) is always positive. Therefore, to satisfy the condition given in (21), sign of $term_2$ in (26) should be positive. The term (x1) in (26) is always positive, so the control gain k_1 must be positive to satisfy the stability condition given in (21).

B. Modeling and control design for WT

As shown in Fig.1, stator terminals of PMBLDCG are connected to the DC bus through a diode rectifier and boost converter used to achieve the MPPT. Using this configuration, the WT voltage varies slightly with variation of the rotor speed, which makes possible to achieve MPPT without measuring rotor position or wind speed.

1) Mathematical model of PMBLDCG

The mathematical model of PMBLDCG is as follows [30],

$$\left[v_{sabc}\right] = R_s\left[i_{sabc}\right] + (L_s - M)\left[di_{sabc}/dt\right] + \left[e_{abc}\right] \tag{27}$$

where v_{sabc}, i_{sabc}, R_s, L_s, M, e_{abc}, denote terminal voltages and currents, stator resistances, inductances, mutual inductance and the back-emf of PMBLDCG, respectively.

The electromagnetic torque of PMBLDCG, is described as,

$$T_e = \left(1/\omega_r\right)\left(e_a i_{WTa} + e_b i_{WTb} + e_c i_{WTc}\right) \tag{28}$$

where ω_r is the mechanical rotor speed and is defined as,

$$\omega_r = (2/P)\,\omega_e \tag{29}$$

where ω_e and P denote the electrical frequency and the number of rotor poles, respectively.

The equation of motion of PMBLDCG is defined as,

$$T_m = T_e + J\left(d\omega_r/dt\right) + B\omega_r \tag{30}$$

where J, B, T_m and T_e denote the moment of inertia, friction coefficient, developed torque and electromagnetic torque, respectively.

2) Mathematical model of the boost converter-2

From Fig.1, a boost converter of WT, is modeled as follows.

For, S_{BWT}=1 (ON),

$$L_2\left(\partial i_{L2}/\partial t\right) = v_{WT} \tag{31}$$

$$C_{out2}\left(\partial v_{out2}/\partial t\right) = -v_{out2}/R \tag{32}$$

$$i_{CWT} = C_{WT}\left(\partial v_{CWT}/\partial t\right) = i_{WT} - i_{L2} \tag{33}$$

And for S_{BWT} =0 (OFF),

$$L_2\left(\partial i_{L2}/\partial t\right) = v_{WT} - v_{out2} \tag{34}$$

$$C_{out2}\left(\partial v_{out2}/\partial t\right) = i_{WT} - \left(v_{out2}/R\right) \tag{35}$$

where S_{BWT}, L_2, C_{WT} ,C_{out2}, R, i_{L2}, i_{WT}, i_{CWT}, v_{out2}, and v_{CWT} represent switch, inductance, input and output capacitances, equivalent load resistance, inductor current, output PV current, input capacitor current, output voltage, and input capacitor voltage of the boost converter-2, respectively.

Based on (31) to (35), the following equations for boost converter-2, are obtained as,

$$\begin{aligned}\left(\partial(i_{WT} - i_{CWT})/\partial t\right) &= \left(\partial(i_{WT} - C_{WT}\partial v_{WT})/\partial t\right) \\ &= \left(v_{WT}/L_2\right) - \left(1-d_2\right)\left(v_{out2}/L_2\right)\end{aligned} \tag{36}$$

$$\left(\partial v_{out2}/\partial t\right) = \left(1/C_{out2}\right)\left[\left(i_{WT}\left(1-d_2\right)\right) - \left(v_{out2}/R\right)\right] \tag{37}$$

Rearranging (36), following expression is obtained,

$$\left(\partial i_{WT}/\partial t\right) = \overbrace{\left(v_{WT}/L_2\right) - \left(1-d_2\right)\left(v_{out2}/L_2\right)}^{Term1} + \overbrace{C_{WT}\left(\partial^2 v_{WT}/\partial t^2\right)}^{Term2} \tag{38}$$

where d_2 is the desired control.

The variation of the v_{WT} during this duration is equal to zero. However, the second derivative of v_{WT} is also equal to zero. Hence, (37) becomes as follows,

$$\left(\partial i_{WT}/\partial t\right) = \left(v_{WT}/L_2\right) - \left(1-d_2\right)\left(v_{out2}/L_2\right) \tag{39}$$

3) Control strategy for boost converter-2

An improved P&O method based SMC with boundary layer, is presented in Fig.3, which is developed to achieve high performance from WT driven variable speed PMBLDCG without mechanical sensors. It is also used to ensure stability at the operating point in finite time, during sudden change in wind speed. For this method, only output (v_{out2}) and input (v_{WT}) DC voltages and the inductor current (i_{L2}) which is equal to the output WT current (i_{WT}), are sensed to obtain the desired control d_2.

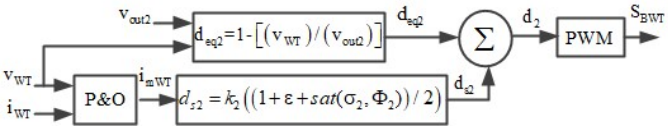

Fig. 3. Improved P&O based SMC with boundary layer for WT.

4) Sliding surface selection

The selected sliding surface σ_2 is designated as,

$$\sigma_2 = \left(\partial P_{dcWT}/\partial i_{WT}\right) = 0 \tag{40}$$

where i_{WT} denotes the DC current and P_{dcWT} is the generated power from WT, which is calculated at the DC side as;

$$P_{dcWT} = v_{WT} i_{WT} \tag{41}$$

Replacing (40) into (41), one gets the following expression as,

$$\sigma_2 = v_{WT} + i_{mWT}\left(\partial v_{WT}/\partial i_{mWT}\right) \tag{42}$$

where i_{mWT} denotes the optimal current obtained using classical P&O method.

5) Determination of the equivalent control

The structure of the desired control (d_2) is expressed as,

$$d_2 = d_{eq2} + d_{s2} \tag{43}$$

And the switching control (d_{s2}) is defined as,

$$d_{s2} = k_2\left(\left(1+\varepsilon+sat(\sigma_2,\Phi_2)\right)/2\right) \tag{44}$$

With

$$sat\left(\sigma_2,\Phi_2\right)\begin{cases} 1 & \sigma_2 \succ \Phi_2 \\ \sigma_2/\Phi_2 & \left|\sigma_2\right| \le \Phi_2 \\ -1 & \sigma_2 \prec -\Phi_2 \end{cases} \tag{45}$$

where k_2 d_{eq2} and Φ_2, denote the control gain, equivalent control, and sliding layer, which is chosen to be between 0.5 and -0.5.

The equivalent control is obtained by setting the derivative of (42) equal to 0.

$$\begin{aligned}\left(\partial\sigma_2/\partial t\right)&=\left(\partial\sigma_2/\partial i_{mWT}\right)\left(\partial i_{mWT}/\partial t\right)\\&=\left(\partial\sigma_2/\partial i_{mWT}\right)\left[\left(v_{WT}/L_2\right)-\left(1-d_2\right)\left(v_{out2}/L_2\right)\right]=0\end{aligned}\tag{46}$$

The non-trivial solution of (46) is expressed as,

$$\left(v_{WT}-(1-d_2)v_{out2}\right)=0\tag{47}$$

The equivalent control is obtained from (47) as,

$$d_{eq2}=1-\left(v_{WT}/v_{out2}\right)\tag{48}$$

6) System stability analysis

The Lyapunov function candidate is used to verify the system stability as,

$$V_2=\left(1/2\right)\sigma_2{}^2\tag{49}$$

The system is said globally stable if the sign of the derivative of (49) is negative as,

$$\left(\partial V_2/\partial t\right)=\sigma_2\left(\partial\sigma_2/\partial t\right)\langle 0\tag{50}$$

Replacing (42) and its derivative expressed in (46) into (50), one obtain following expression,

$$\begin{aligned}\left(\partial V_2/\partial t\right)=&\overbrace{\left(v_{WT}+i_{mWT}\left(\partial v_{WT}/\partial i_{mWT}\right)\right)}^{Term1}\\&\overbrace{\left(2\left(\partial v_{WT}/\partial i_{mWT}\right)+i_{mWT}\left(\partial^2 v_{WT}/\partial^2 i_{mWT}\right)\right)}^{Term2}\\&\overbrace{\left(\left(v_{WT}/L_2\right)-(1-d_2)\left(v_{out2}/L_2\right)\right)}^{Term3}\langle 0\end{aligned}\tag{51}$$

It is observed that the three terms in (51) are depending on v_{WT}. Neglecting semiconductor voltage drops, as well as, commutation overlaps, an output DC (v_{WT}) voltage is defined as [31],

$$v_{WT}=2k_m\omega_r\tag{52}$$

where k_m is motor back EMF constant and ω_r is the rotor mechanical speed, which is obtained using an experimental characteristic of PMBLDCG given in Table I and depicted in Fig.4.

TABLE I

EXPERIMENTAL CHARACTERISTIC OF THE PMBLDCG

i_{WT}(A)	0.290	1.9	3.7	5.3
ω_r(RPM)	451	501	551	601

The relationship that expresses the mechanical rotor speed of PMBLDCG versus the output DC current (i_{WT}) is expressed as follows,

$$\omega_r=3.1i_{mWT}+46\tag{53}$$

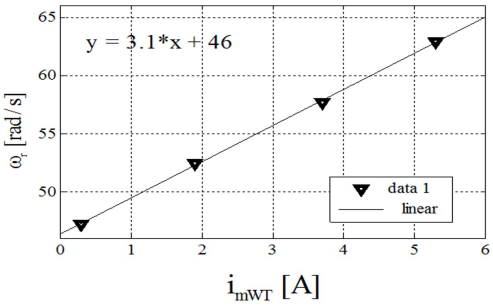

Fig. 4 Experimental characteristic $\omega_r=f(i_{mWT})$ of PMBLDCG.

Replacing (53) into (52), one obtains following expression as,

$$v_{WT}=k_m\left(6.2i_{mWT}+92\right)\tag{54}$$

To satisfy the stability condition given in (50) the sign of each term in (51) is verified separately.

Using (54), one determines the sign of the 1st and 2nd derivative of v_{WT}.

$$k_m\partial\left(6.2i_{mWT}+92\right)/\partial i_{mWT}=6.2k_m\rangle 0\tag{55}$$

$$k_m\partial^2\left(6.2i_{mWT}+92\right)/\partial^2 i_{mWT}=0\tag{56}$$

Replacing (55) and (56) into the $term_1$ and $term_2$ of (51), we obtain the following expressions as,

$$k_m\left(6.2i_{mWT}+92\right)+6.2k_m i_{mWT}\rangle 0\tag{57}$$

Moreover,

$$12.4k_m+0\rangle 0\tag{58}$$

It is clear that the sign of $term_1$ and $term_2$ of (51) are positive. Therefore, the sign of the $term_3$ must be negative in order to satisfy the stability condition.

Replacing (44) and (48) into $term_3$ of (51), one obtains the following expression as,

$$\overbrace{\left(v_{out2}/L_2\right)}^{Term1}\overbrace{k_2\left(\left(1+\varepsilon+sat(\sigma_2,\Phi_2)\right)/2\right)}^{Term2\;\;x2}\langle 0\tag{59}$$

The sign of the $term_1$ in (58) is always positive. Therefore, to satisfy the stability condition given in (50), sign of $term_2$ in (59) must be negative. The term (x2) in (59) is always positive, so the control gain (k_2) must be negative to satisfy the stability condition.

C. Modeling and control design of three-phase inverter

Fig.5 shows the control scheme of the APC based on AWPI controller for the AC voltage regulation. The system frequency is maintained constant by operating the DC-AC interfacing inverter at 60Hz. Applying Kirchhoff's voltage and current laws at the connection point of the three-phase interfacing inverter shown in Fig.1, following differential equations in natural three-phase coordinate system (a-b-c), are obtained as,

$$\left(di_{inv(abc)}/dt\right)=\left(1/L_f\right)\left(d_{(abc)}V_{dc}-v_{L(abc)}\right)\tag{60}$$

$$\left(dv_{L(abc)}/dt\right)=\left(1/C_f\right)\left(i_{inv(abc)}-i_{L(abc)}\right)\tag{61}$$

where $d_{(abc)}$, v_{Labc}, $i_{inv(abc)}$, $i_{L(abc)}$, V_{dc}, C_f and L_f represent the control variable, AC voltages, output inverter currents, load currents, DC link voltage, capacitance and inductance of the inverter output filter, respectively.

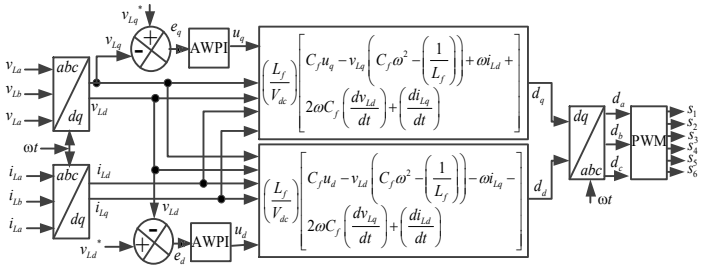

Fig. 5 APC based AWPI controller for DC-AC interfacing inverter.

This article has been accepted for publication in a future issue of this journal, but has not been fully edited. Content may change prior to final publication. Citation information: DOI 10.1109/TIE.2017.2777404, IEEE Transactions on Industrial Electronics

Applying Park's transformation to (60) and (61), one obtains the following expressions in d, q rotating frame as,

$$\begin{cases} \left(di_{invd}/dt\right) = \left(V_{dc}/L_f\right)d_d + i_{invq}\omega + v_{Ld} \\ \left(di_{invq}/dt\right) = \left(V_{dc}/L_f\right)d_q - i_{invd}\omega + v_{Lq} \end{cases} \quad (62)$$

$$\begin{cases} \left(dv_{Ld}/dt\right) = \left(1/C_f\right)\left(i_{invd} - i_{Ld}\right) + \omega v_{Lq} \\ \left(dv_{Lq}/dt\right) = \left(1/C_f\right)\left(i_{invq} - i_{Lq}\right) - \omega v_{Ld} \end{cases} \quad (63)$$

Replacing (62) in the derivative of (63), one gets the following expressions,

$$\begin{cases} C_f\overbrace{\left(d^2v_{Lq}/dt^2\right)}^{u_q} = v_{Lq}\left(C_f\omega^2 - \left(1/L_f\right)\right) - \\ 2\omega C_f\left(dv_{Ld}/dt\right) + \left(V_{dc}/L_f\right)d_q - \omega i_{Ld} - \left(di_{Lq}/dt\right) \\ C_f\overbrace{\left(d^2v_{Ld}/dt^2\right)}^{u_d} = v_{Ld}\left(C_f\omega^2 - \left(1/L_f\right)\right) + \\ 2C_f\omega\left(dv_{Lq}/dt\right) + \left(V_{dc}/L_f\right)d_d + \omega i_{Lq} - \left(di_{Ld}/dt\right) \end{cases} \quad (64)$$

where u_d and u_q denote new equivalent inputs, and ω is pulsation, which is defined as,

$$\omega = 2\pi f_s \quad (65)$$

where f_s denotes the system frequency and is set equal to 60Hz.

From (64), one extracts the control laws d_d and d_q as,

$$\begin{cases} d_q = \left(L_f/V_{dc}\right)\begin{bmatrix} C_f u_q - v_{Lq}\left(C_f\omega^2 - \left(1/L_f\right)\right) + \omega i_{Ld} \\ +2\omega C_f\left(dv_{Ld}/dt\right) + \left(di_{Lq}/dt\right) \end{bmatrix} \\ d_d = \left(L_f/V_{dc}\right)\begin{bmatrix} C_f u_d - v_{Ld}\left(C_f\omega^2 - \left(1/L_f\right)\right) - \omega i_{Ld} \\ -2\omega C_f\left(dv_{Lq}/dt\right) + \left(di_{Ld}/dt\right) \end{bmatrix} \end{cases} \quad (66)$$

The dq-axis AC voltages v_{Ld} and v_{Lq} are controlled independently by acting upon the inputs u_d and u_q, respectively. However, the tracking controllers, are obtained as follows [32],

$$\begin{cases} u_q = \left(k\tau_C\left(\tau_i s+1\right)/\tau_i\left(\tau_C s+1\right)\right)e_q + \left(1/\left(\tau_C s+1\right)\right)u_{q\max} \\ u_d = \left(k\tau_C\left(\tau_i s+1\right)/\tau_i\left(\tau_C s+1\right)\right)e_d + \left(1/\left(\tau_C s+1\right)\right)u_{d\max} \end{cases} \quad (67)$$

where $e_{d,q}$, $v_{Ld,q}$,k ,τ_i,and τ_C denote the dq-axis AC voltage error, dq-axis AC voltages, proportional, integral feedback gain coefficients, respectively.

Fig. 6 shows the block diagram for AWPI controller with feedback path control for d and q axis to avoid the saturation problem. The AWPI controller model is based on time constants τ_c and τ_i, as well as, the gain k, which have a visible effect on system performance when saturation occurs. Therefore, to get high performance, optimal gains design is required. The selected optimal gain values are given in Table II of Appendix.

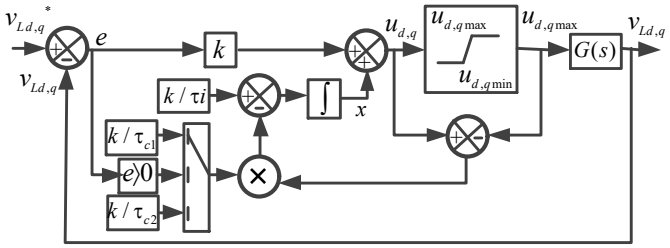

Fig. 6 Block diagram of the AWPI controller with feedback path control for d and q axis.

IV. Simulation and Experimental Results

Performance of the APC based AWPI controller and improved P&O based SMC with boundary layer developed in this work are simulated under severe conditions using Matlab/Simulink and validated in real time using hardware prototype built in the laboratory.

A. Performance of improved P&O based SMC with boundary layer for WT and SPVA under weather change

Fig. 7 (a) shows the waveforms of the mechanical torque (T_m), rotor speed of PMBLDCG (ω_r), stator voltage (v_{sa}) and current (i_{sa}) of phase "a", the output DC voltage (v_{WT}), output DC current (i_{WT}), inductor current (i_{WT}=i_{L2}), the current reference (i_{mWT}) and the desired control (d_2). It is observed that i_{sa} and i_{WT} vary with variation of T_m developed by WT, the v_{sa} and v_{WT} vary slightly during variation of ω_r compared to its rated values. It is clearly observed that i_{WT} varies with variation of ω_r, with increments at t = 0.4 s, 0.9 s and 1.4 s. The i_{WT} (which is equal to the i_{L2}), follows its reference i_{mWT} during sudden variation and MPPT is achieved without measurement of ω_r or wind speed. Furthermore, the control d_2 remains within the defined range of variation even during transition and simultaneous operation of boost converter-1 and three-phase interfacing inverter, which confirms the robustness of the improved P&O method.

In Fig. 7 (b) the waveforms of the solar insolation, output PV voltage (v_{PV}), output PV current (i_{PV}), inductor current (i_{L1}) and PV current reference (i_{mPV}) and the control (d_1), are presented. The solar insolation is increased at t=0.3s, decreased at t=0.8s and increased again at t=1.3s. It is observed that i_{L1} follows its reference during increase and decrease in solar insolation. MPPT from SPVA is achieved quickly without control divergence. However, d_1 is not affected due to variation of solar insolation and simultaneously operation of boost converter-2, and the interfacing inverter. It is staying within the defined range during transient and steady state conditions. This confirms the robustness of the improved P&O based SMC with boundary layer.

B. Performance of the APC based AWPI controller under different type of loads

Fig. 8 (a) shows the waveforms of the DC link voltage (V_{dc}), which is equal to battery voltage (V_{bat}), AC voltage (v_L) and load current (i_L), and the system frequency (fs) during: a) steady-state, b) sudden increased in linear load at t=0.1s, c) phase "a" load is switched ON between t=0.03s and t=0.13s,

This article has been accepted for publication in a future issue of this journal, but has not been fully edited. Content may change prior to final publication. Citation information: DOI 10.1109/TIE.2017.2777404, IEEE Transactions on Industrial Electronics

and d) presence of balanced and unbalanced nonlinear load. This test is performed under load and weather condition change. One can see clearly that APC based AWPI controller performs well during sever conditions, such as disconnected load in Fig.8 (b) between t=0 s and t=0.1s and during presence of unbalance linear load in Fig.8 (c), as well as balanced and unbalanced nonlinear load in Fig.8 (d).

It is observed in Figs.8 (a-d) that the AC voltage is regulated constant and sinusoidal with zero steady state error. It is demonstrated that APC performs well under different conditions. Furthermore it is proven that AWPI controller perform well during transient and steady state without any saturation and control divergence. This confirms the robustness of the APC based on AWPI controller with optimal gains design.

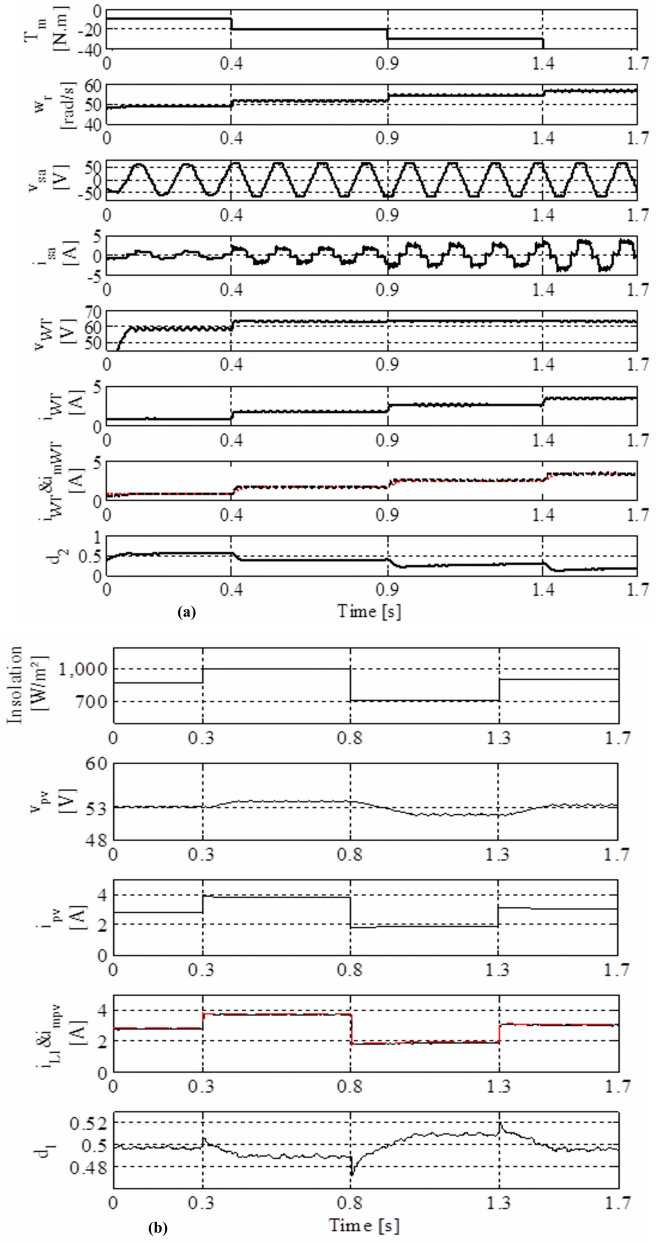

Fig. 7. a) Obtained results of improved P&O based SMC with boundary layer WT side, and b) SPVA side.

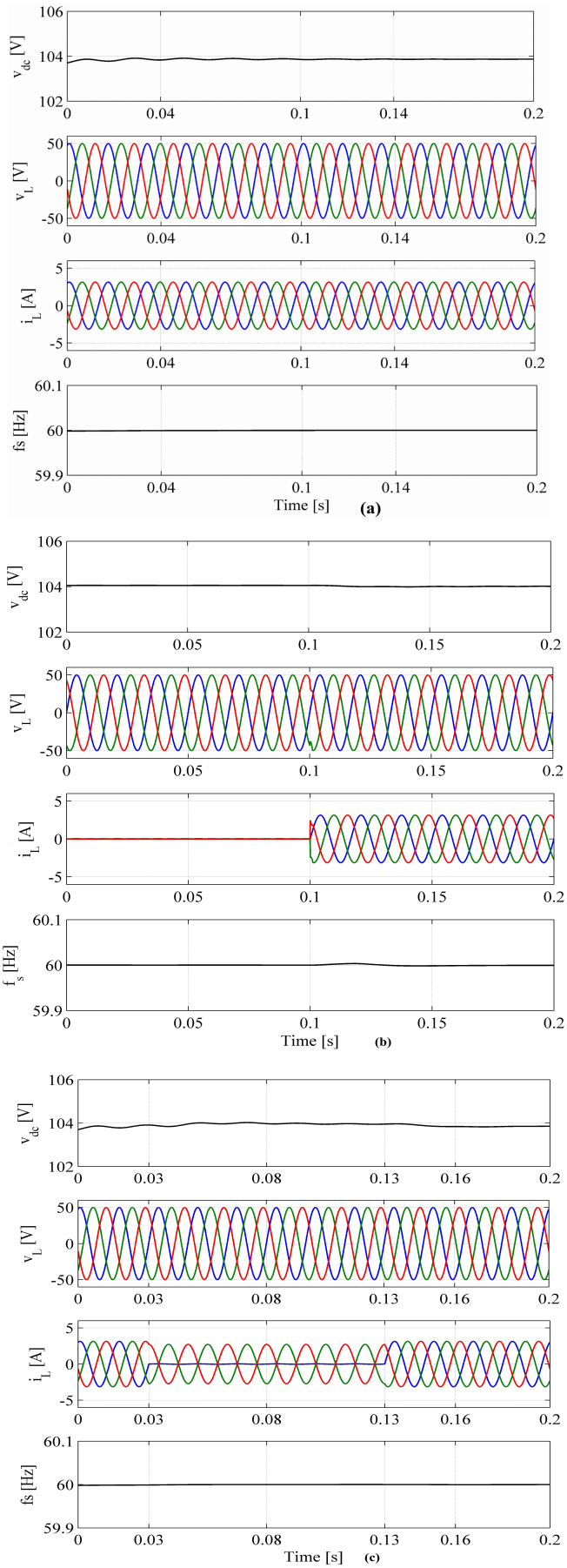

This article has been accepted for publication in a future issue of this journal, but has not been fully edited. Content may change prior to final publication. Citation information: DOI 10.1109/TIE.2017.2777404, IEEE Transactions on Industrial Electronics

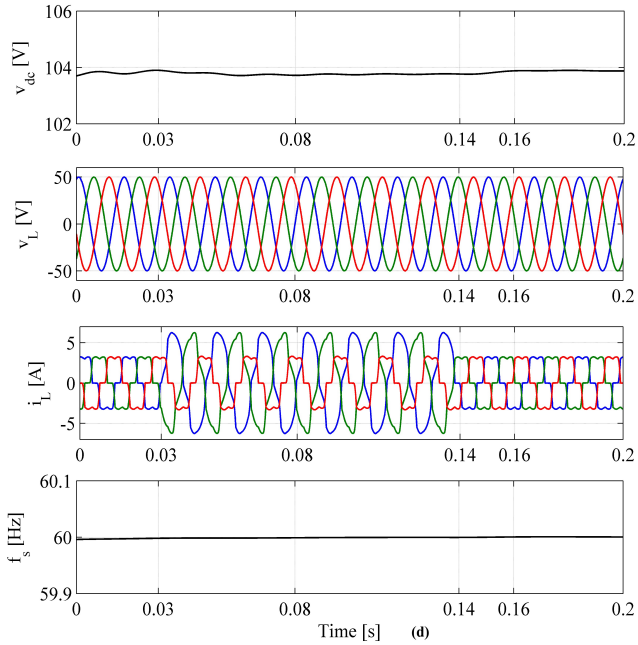

Fig.8. Performance of the APC based AWPI controller under a) steady-state, b) sudden increased of load at t=0.1s, c) unbalance linear load, and d) balanced and unbalanced nonlinear load.

C. Experimental Results

Fig. 9 shows an experimental configuration used to validate in real time the HSPGS configuration and the developed control strategies. It consists of Lab-Volt WT emulator coupled with PMBLDCG and Lab-Volt PV emulator, Semikron power converter, voltage and current sensors, lead acid batteries, isolated card and DSP-dSPACE real time controller.

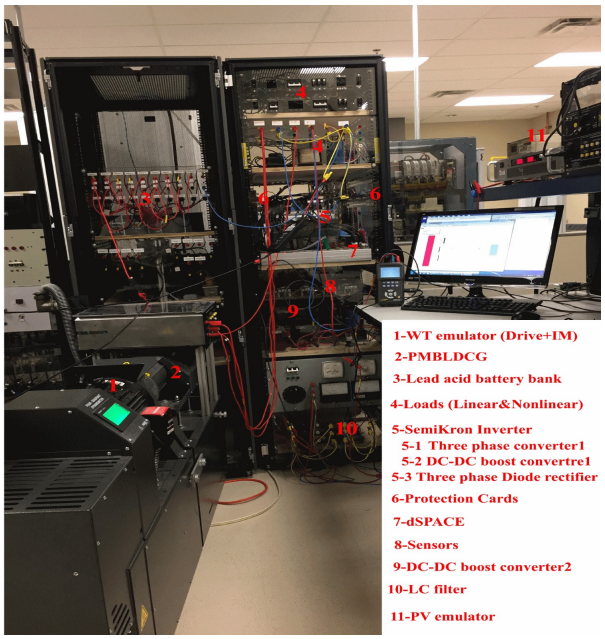

Fig. 9. Experimental hardware configuration of HSPGS.

1) Test of the APC based AWPI controller at load variation

In Fig.10 (a-d) the waveforms of the line-neutral AC voltages (v_{La}, v_{Lc}) and load currents (i_{La}, i_{Lc}), are shown. To study the performance of the APC and its AWPI voltage controller, system is subjected to: a) sudden increasing in load at t=0.05s (Fig.10.a), b) phase (c) is disconnected at =0.05s (Fig.10.b), c) no load at t=0.05s (Fig.10.c), and d) balanced nonlinear load (Fig.10.d). It is observed that AC voltage is regulated constant and sinusoidal in presence of all conditions. One can see clearly that AWPI controller acts quickly during transition without voltage overshoot, which confirms the robustness of the controller for voltage regulation in standalone system.

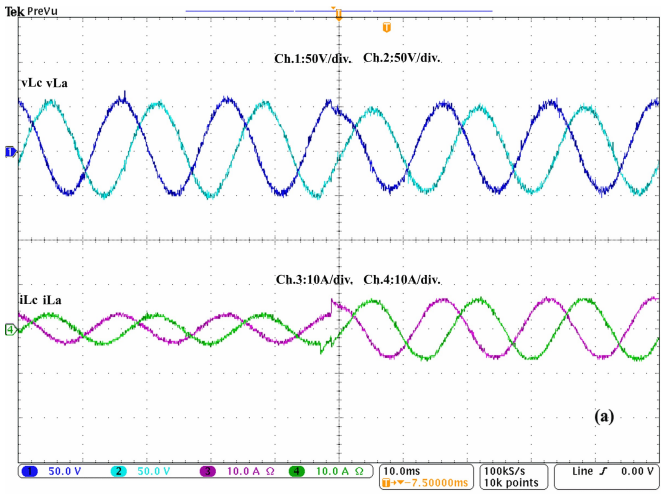

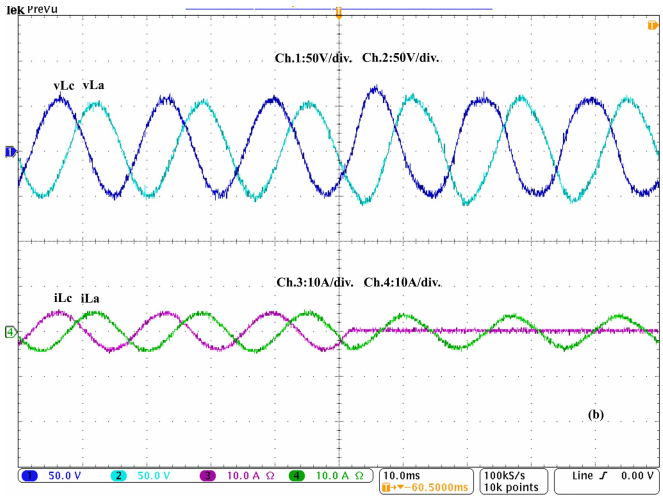

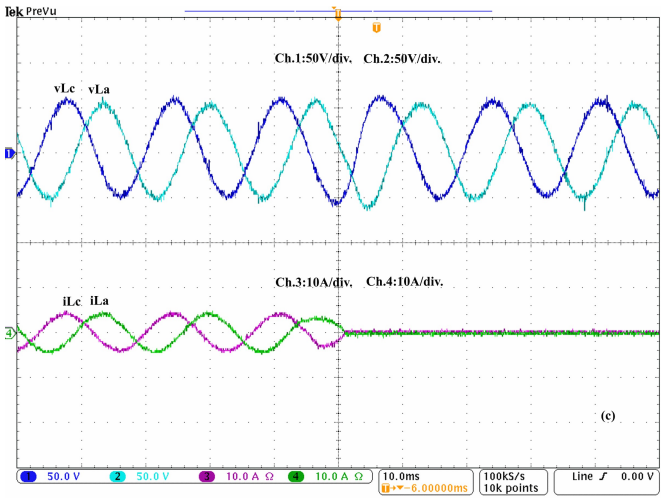

This article has been accepted for publication in a future issue of this journal, but has not been fully edited. Content may change prior to final publication. Citation information: DOI 10.1109/TIE.2017.2777404, IEEE Transactions on Industrial Electronics

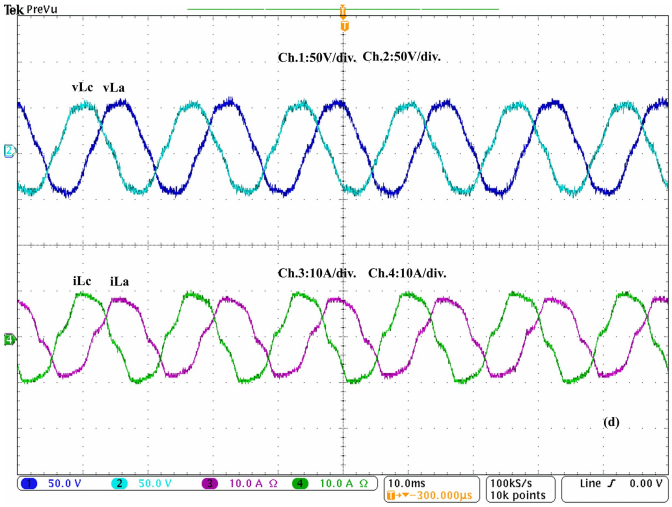

Fig. 10. Performance of the APC based AWPI controller under: a) dynamic linear load change, b) removed of one phase, c) complete removed of load, and d) balanced nonlinear load.

2) Test results of P&O based SMC with boundary layer under weather change

In Fig.11 (a) the waveforms the stator phase voltage (v_{sa}) and current (i_{sa}), and output DC voltage (v_{WT}) and current (i_{WT}), are presented. To study the performance of improved P&O based SMC with boundary layer to achieve MPPT from variable speed WT coupled with PMBLDCG without speed measurement, the system is subjected to wind speed variation at t=0.8s, and at t=2.8s. It is observed that v_{WT} vary slightly with variation of the wind speed but i_{sa} and i_{WT} are increased at t=0.8s and increased further at t=2.8s without control divergence during transition period.

In Fig.11 (b), the waveforms of the line AC voltage (v_{Lab}), load current (i_{La}), output PV current (i_{PV}), and battery current (i_{bat}), are presented. To study the performance of the improved P&O based SMC with boundary layer to achieve MPPT from SPVA, the system is subjected to different insolations at t=0.2 s and t=0.6s. It is observed that the system performs well without any divergence in control during transition when several power converters operate simultaneously. This confirms the robustness of the control approach for MPPT when several power converters operate simultaneously.

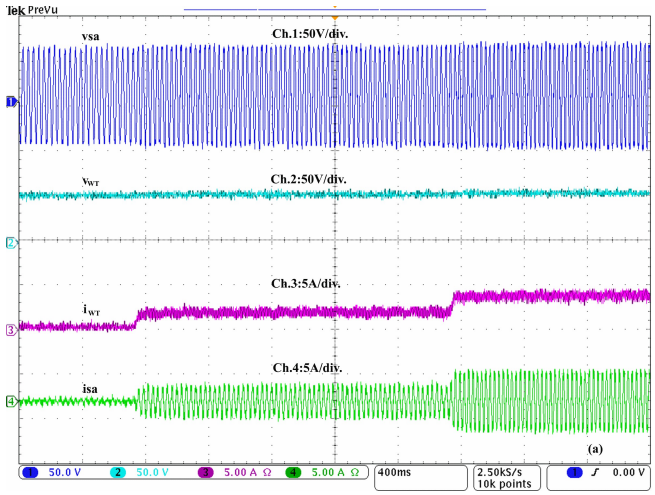

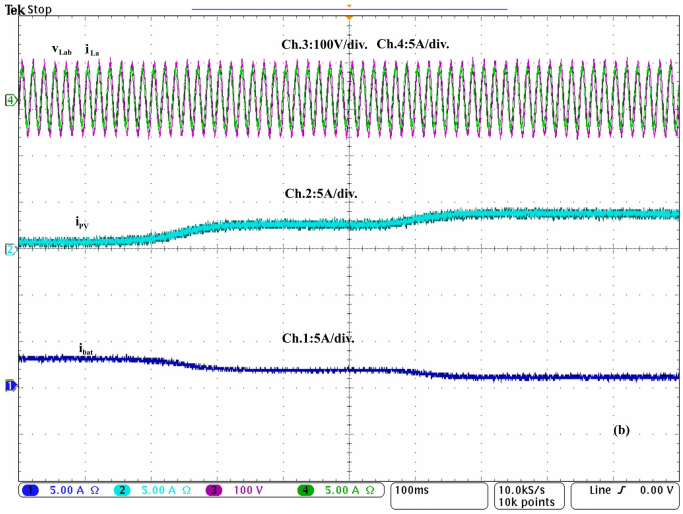

Fig. 11. Test of improved P&O based SMC with boundary layer under a) wind speed, and) solar insolation change.

3) Test results at fixed linear load and variation in weather conditions

The waveforms of the line to neutral AC voltage (v_{La}), battery current (i_{bat}), output PV current (i_{PV}) and WT output DC current (i_{WT}), are presented in Fig. 12. The performance of the system is obtained when all power converters operate together to fulfill a fixed linear load by applying the following conditions: a) absence of solar insolation and wind speed in the beginning and sudden increase of wind speed, b) absence of solar insolation and sudden decrease of the wind speed, c) absence of wind speed and sudden decrease of the insolation, d) presence of the wind speed and insolation at the beginning and sudden decrease of insolation. In all tests load is kept constant. It is observed that AC voltage is regulated constant and sinusoidal with zero steady state error during transient operations. Further, it is observed that BESS current varies with variation of output PV and WT currents, it balances the power in the system by charging and discharging the battery. It is observed that P&O based SMC perform well when many power converters operate simultaneously. Furthermore, the APC with AWPI controller is able to maintain the AC voltage constant and sinusoidal in the presence of different conditions.

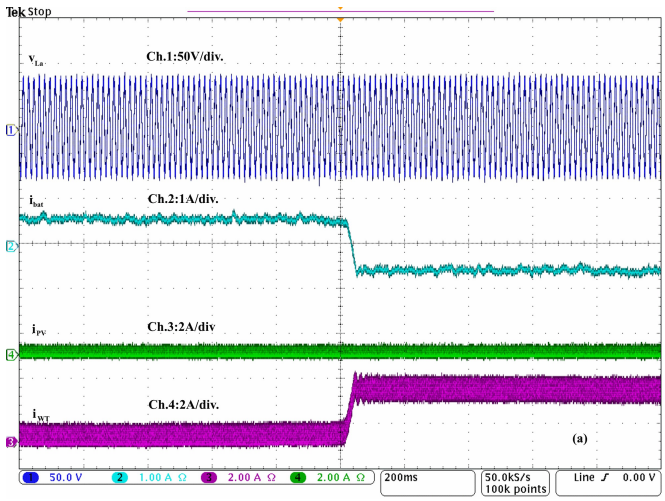

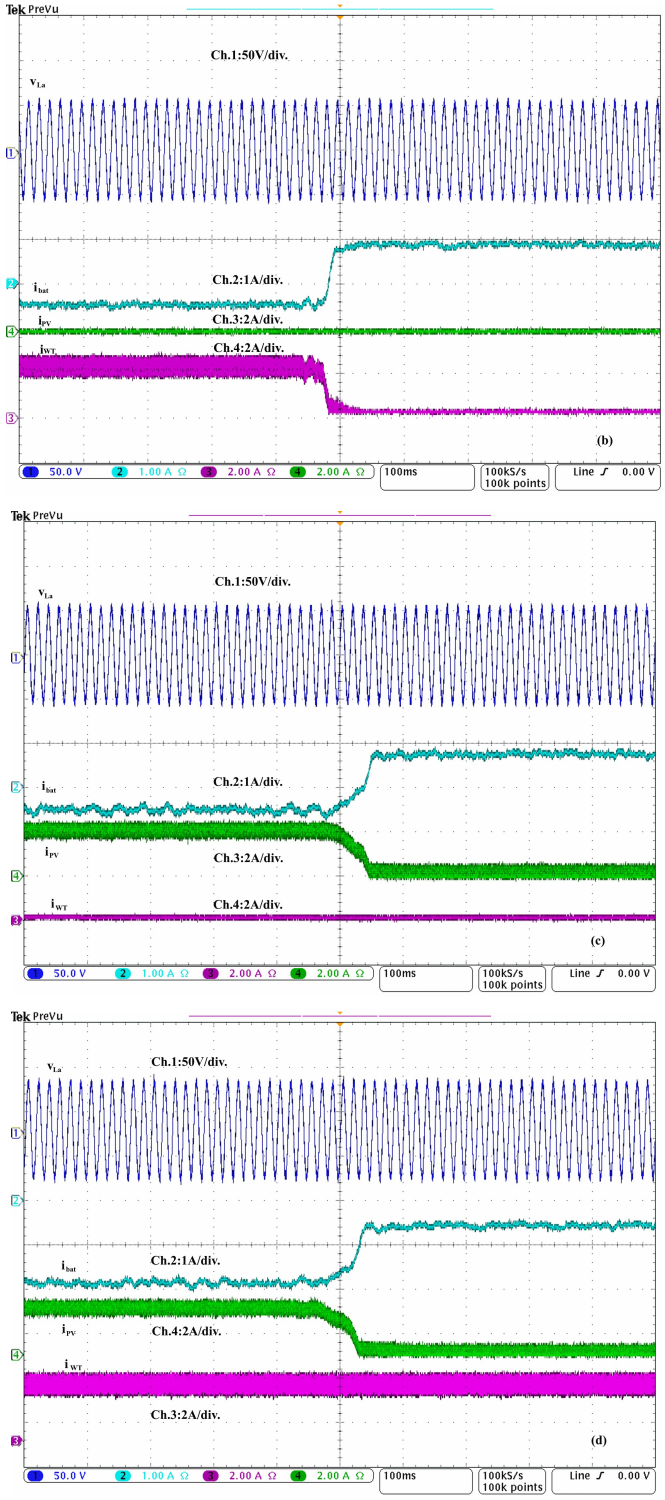

Fig.12. Dynamic performance under wind and solar insolation change.

I. Conclusion

A wind-PV-battery based hybrid power generation system has been proposed for standalone application. Modeling, control design, and stability analysis have been presented in detail. Simulated performance of the system has been obtained with an improved P&O method for MPPT of SPVA and WT. For a multiple source power generation system, SMC with boundary layer is designed for improved performance under variable weather conditions. It has been demonstrated that the improved P&O based MPPT is more reliable and efficient during weather changes in presence of many power converters operated simultaneously. Further, it has been demonstrated that the APC with AWPI voltage controller regulates constant and sinusoidal AC voltage without any saturation and overshoot during transients. Simulated performance has been validated on real-time laboratory prototype for improved P&O based SMC with boundary layer and the APC with AWPI controller with reduced number of sensors and hardware complexity.

Appendix

TABLE II

SYSTEM PARAMETERS

Element	Parameters
SPVA side	i_{rr}=5.981. 10^{-8} A, i_{scr}=6 A, k_i=0.0024, Tr=298 K q=1.6. 10^{-19} C, K_b=1.38. 10^{-23} J/K, E_g=1.12 V, A=1.2 C_{out1}=1000μF, C_1=1000 μF, L_1=1.5 mH, k_1=50
WT side	R_s=0.808 Ω, L_s=5.44 mH, V_s=208 V, ω_r= 1800 RPM, L_{WT}=1.5 mH,, J=0.01859 kg.cm^2, K_m=80 V/tr/min, C_{out2}=1000μF, C_2=1000 μF, 2P=4, k_2=50
DC Bus	C_{dc}=2500 μF, V_{dc}=105 V, lead acid batteries 9*(12V/12) Ah.
AC Side	f_s=60 Hz, V_{LL}=50V, L_f=5mH, C_f= 40 μF linear load (R_L=8 Ω), nonlinear load (R_L=8 Ω, L_L=20 mH), k=3, τ_{c1}=0.5, τ_{c2}=10, τ_t=2

References

[1] D. Li and Z. Q. Zhu, "A Novel Integrated Power Quality Controller for Microgrid," *IEEE Trans. Ind. Electr*, vol. 62, no5, pp. 48-58, May 2015.

[2] H. Lotfi and A. Khodaei, "AC Versus DC Microgrid Planning," *IEEE Trans. Smart Grid*, vol. 8,no1, pp. 296-304, Jan. 2017.

[3] A. C. Luna, N. L. D. Aldana, M. Graells, J. C. Vasquez, and J. M. Guerrero, "Mixed-Integer-Linear-Programming based Energy Management System for Hybrid PV-wind-battery Microgrids: Modeling, Design and Experimental Verification," *IEEE Trans. Power Electro.* vol. 32, no4, pp. 2769-2783, April 2017.

[4] L. Minchala-Avila, L. Garza-Castanon, Y. Zhang, and H. Ferrer, "Optimal Energy Management for Stable Operation of an Islanded Microgrid," *IEEE Trans. Ind. Inf*, vol. 12, pp. 1361-1370, Aug. 2016.

[5] J. M. Guerrero, P. C. Loh, T. L. Lee, and M. Chandorkar, "Advanced Control Architectures for Intelligent Microgrids-;Part II: Power Quality, Energy Storage, and AC/DC Microgrids," *IEEE Trans. Industrial Electro.*, vol. 60,no 4, pp. 1263-1270, April 2013.

[6] Y. Yang, F. Blaabjerg, H. Wang, M. G. Sim, "Power control flexibilities for grid-connected multi-functional photovoltaic inverters," *IET Renewable Power Generation*, vol. 10, no 4, pp. 504-513, April 2016.

[7] C. Cecati, F. Ciancetta, and P. Siano, "A Multilevel Inverter for Photovoltaic Systems with Fuzzy Logic Control," *IEEE Trans. Ind. Electon.*, vol. 57, no57, pp. 4115-4125, Dec.2010.

[8] L. Zhang, X. Ruan, and X. Ren, "Second-Harmonic Current Reduction and Dynamic Performance Improvement in the Two-Stage Inverters: An Output Impedance Perspective," *IEEE Trans. Ind. Electron.*, Jan.2015.

[9] M. Rezkallah, A. Hamadi, A. Chandra, and B. Singh, "Real-Time HIL Implementation of Sliding Mode Control for Standalone System Based on PV Array Without Using Dump-load," *IEEE Trans. Sustainable Energy*, Oct. 2015.

[10] Y. Zhu, J. Yao, and D. Wu, "Comparative study of two stages and single stage topologies for grid-tie photovoltaic generation by PSCAD/EMTDC," in *Proc. APSA and Protection*, 2011, pp. 1304-1309.

[11] M. A. G. d. Brito, L. Galotto, L. P. Sampaio, G. d. A. e. Melo, and C. A. Canesin, "Evaluation of the Main MPPT Techniques for Photovoltaic Applications," *IEEE Trans. Ind. Electron.,* vol. 60, no 3, pp.56-67, March 2013.

[12] K. H. Kim, T. L. Van, D. C. Lee, S. H. Song, and E. H. Kim, "Maximum Output Power Tracking Control in Variable-Speed Wind Turbine Systems

Considering Rotor Inertial Power," *IEEE Trans. Ind. Electron.*, vol.60, no8, pp. 3207-3217, Aug. 2013

[13] J. Ahmed and Z. Salam, "A Modified P&O Maximum Power Point Tracking Method with Reduced Steady State Oscillation and Improved Tracking Efficiency," *IEEE Trans. Sus. Energy,* vol. 7, no4, pp 1506-1515, Oct.2016.

[14] X. Li, H. Wen, L. Jiang, W. Xiao, Y. Du, and C. Zhao, "An Improved MPPT Method for PV system with Fast-Converging Speed and Zero Oscillation," *IEEE Trans. Ind. Applications*, vol. 52, no 6, pp. 5051-5064, Dec. 2016.

[15] A. Pandey, N. Dasgupta, and A. K. Mukerjee, "High-Performance Algorithms for Drift Avoidance and Fast Tracking in Solar MPPT System," *IEEE Trans. Energy Conversion*, vol. 23, no 2, pp. 681-689, June 2008.

[16] E. Mamarelis, G. Petrone, and G. Spagnuolo, "An Hybrid Digital-Analog Sliding Mode Controller for Photovoltaic Applications, " *IEEE Trans. Ind. Informatics*, vol. 9, no2, pp. 1094-1103, May 2013.

[17] Y. Levron and D. Shmilovitz, "Maximum Power Point Tracking Employing Sliding Mode Control, "*IEEE Transactions on Circuits and Systems I: Regular Papers*, vol. 60, no3, pp. 724-732, March 2013.

[18] B. Beltran, T. Ahmed-Ali, and M. E. H. Benbouzid, "Sliding Mode Power Control of Variable-Speed Wind Energy Conversion Systems, " *IEEE Trans. Energy Conversion*, vol. 23, no2, pp. 551-558, June 2008.

[19] S. F. Toloue and M. Moallem, "Multivariable Sliding-Mode Extremum Seeking Control With Application to MPPT of an Alternator-Based Energy Conversion System, " *IEEE Trans. Ind. Electro.*, vol. 64, no8, pp. 6383-6391, Aug.2017.

[20] E. Bianconi, J. Calvente, R. Giral, E. Mamarelis, G. Petrone, C. A. Ramos-Paja, et al., "A Fast Current-Based MPPT Technique Employing Sliding Mode Control, "*IEEE Trans. Ind. Electronics*, vol. 60, no3, pp. 1168-1178, March 2013.

[21] M. Rezkallah, S. K. Sharma, A. Chandra, B. Singh, and D. R. Rousse, "Lyapunov Function and Sliding Mode Control Approach for the Solar-PV Grid Interface System, " *IEEE Trans. Ind. Electron.*, vol. 64, no1, pp. 785-795, Jan. 2017

[22] J. W. Jung, N. T. T. Vu, D. Q. Dang, T. D. Do, Y. S. Choi, and H. H. Choi, "A Three-Phase Inverter for a Standalone Distributed Generation System: Adaptive Voltage Control Design and Stability Analysis, " *IEEE Trans.Energy Conversion*, vol. 29, no1, pp. 46-56, March, 2014.

[23] D. Q. Dang, Y. S. Choi, H. H. Choi, and J. W. Jung, "Experimental Validation of a Fuzzy Adaptive Voltage Controller for Three-Phase PWM Inverter of a Standalone DG Unit, " *IEEE Trans. Ind. Informatics*, vol. 11, no3, pp. 632-641, June 2015.

[24] Z. Wang, W. Wu, and B. Zhang, "A Distributed Quasi-Newton Method for Droop-Free Primary Frequency Control in Autonomous Microgrids," *IEEE Trans. Smart Grid*, vol. PP, pp. 1-1, 2016.

[25] Q. C. Zhong, "Robust Droop Controller for Accurate Proportional Load Sharing Among Inverters Operated in Parallel," *IEEE Trans. Ind. Electro.*, vol. 60, no 4, pp. 1281-1290, April 2013.

[26] X. Tang, X. Hu, N. Li, W. Deng, and G. Zhang, "A Novel Frequency and Voltage Control Method for Islanded Microgrid Based on Multienergy Storages," *IEEE Trans. Smart Grid*, vol. 7, no1, pp. 410-419, Jan. 2016.

[27] H. Shi, F. Zhuo, H. Yi, F. Wang, D. Zhang, and Z. Geng, "A Novel Real-Time Voltage and Frequency Compensation Strategy for Photovoltaic-Based Microgrid," *IEEE Trans. Ind. Electro*, vol. 62, no6, pp. 3545-3556, June 2015.

[28] W. Wang, Y. Li, Y. Cao, U. Haeger, and C. Rehtanz, "Adaptive Droop Control of MTDC System for Frequency Support and Power Sharing, " *IEEE Trans. Power Systems*, vol. *Early access*, pp. 1-1, 2017.

[29] J. H. Teng, W. H. Huang, T. A. Hsu, and C. Y. Wang, "Novel and Fast Maximum Power Point Tracking for Photovoltaic Generation," *IEEE Trans. Ind. Electro.*, vol.63, no 8, pp.4955-4966, Aug.2016.

[30] Paul C. Krause Oleg Wasynczuk; Scott D Sudhoff, "Analysis of electric machinery and drive systems," *Wiley-IEEE Press*, 2002, pp. 262-266.

[31] Ion Bodea, "Variable Speed generators," *CTC Press Taylor& Francis Group*,2006, ch10, pp. 35.

[32] M. Yang, L. Niu, and D. g. Xu, "A novel piecewise Anti-Windup design for speed loop PI controller of PMSM servo system," *in Proc. (EPE/PEMC)*. 2012, pp. DS2a.3-1-DS2a.3-5.

Miloud Rezkallah (S'11–M'14) received the B. Tech. degree in electrical machines and drive from the University of Science and Technology USTO (now University Mohamed Boudiaf), Oran, Algeria, and the M. Tech. and Ph.D. degrees in power electronics and system control from École de Technologie Supérieure, Université du Québec, Montréal, Canada., in 2010 and 2016, respectively. He is working as a postdoctoral fellow in Electrical Engineering Department at École de Technologie Supérieure and as researcher at the research center on smart grids and energy systems (CERISE). His research interests include control and design of microgrid, active filters, renewable energy generations and applications, and energy storage systems.

Abdelhamid Hamadi received the Bachelor of Engineering degree in electrical from University of Polytechnics, ENP, Algiers, Algeria, in 1987, and the M.Tech and Ph.D. degrees in power electronic and control from École de Technologie Supérieure, Montreal, QC, Canada, in 2010. Currently, he is working as a research assistant with the Department of Electrical Engineering, École de Technologie Supérieure. His research interests include the application of power electronics in distribution systems, power quality analysis, active power filters, hybrid power filters, series power hybrid filter, passive filters, and renewable energy.

A**mbrish Chandra** (SM'99–F'14) received the Electrical engineering degree from Indian Institute of Technology (IIT), Roorkee, India, in 1977 the M.Tech. degree in power apparatus and systems from the IIT, in1980, and the Ph.D. degree from the University of Calgary, Canada, in 1987. From 2012 to 2015, he was the Director of the graduate program on "renewable energy and energy efficiency" at the École de Technologie Supérieure (ÉTS), Université du Québec, Montréal, QC, Canada, where since 1994, he has been a Professor with the Department of Electrical Engineering. His research interests include power quality, active filters, static reactive power compensation, flexible ac transmission systems (FACTS), and control and integration of renewable energy resources. He has coauthored the book Power Quality—Problems and Mitigation Techniques (Wiley, 2015). He is a Distinguished Lecturer of IEEE Power and Energy Society and also of IEEE Industry Application Society. Dr. Chandra is an Associate Editor of the IEEE Transactions on Industrial Electronics. He is a Professional Engineer in the Province of Quebec, Canada.

Bhim Singh (SM'99, F'10) was born in Rahamapur, Bijnor (UP), India, in 1956. He received his B.E. (Electrical) from the University of Roorkee, India, in 1977 and his M.Tech. and Ph.D. from the IIT Delhi, India, in 1979 and 1983, respectively. In 1983, he joined the Department of Electrical Engineering, University of Roorkee as a Lecturer. He became a Reader there in 1988. In December 1990, he joined the Department of Electrical Engineering, IIT Delhi, India, as an Assistant Professor, where he has become a Professor in 1997. Presently he is Head of the Department of Electrical Engineering at IIT Delhi. Prof. Singh has guided 60 Ph.D. dissertations, 161 M.E./M.Tech./M.S.(R) theses. His areas of research interest include power electronics, electrical machines and drives, renewable energy, active filters, FACTS, HVDC, and power quality.